FULL PAPER

B$_0$ shimming of the human heart at 7T

Michael Hock[1] iD | **Maxim Terekhov**[1] iD | **Maria Roxana Stefanescu**[1] | **David Lohr**[1] iD |
Stefan Herz[1,2] iD | **Theresa Reiter**[1,3] | **Markus Ankenbrand**[1] iD | **Aleksander Kosmala**[1,2] iD |
Tobias Gassenmaier[1,2] iD | **Christoph Juchem**[4,5] iD | **Laura Maria Schreiber**[1] iD

[1]Chair of Cellular and Molecular Imaging, Comprehensive Heart Failure Center (CHFC), University Hospital Wuerzburg, Wuerzburg, Germany

[2]Department of Diagnostic and Interventional Radiology, University Hospital Wuerzburg, Wuerzburg, Germany

[3]Department of Internal Medicine I, University Hospital Wuerzburg, Wuerzburg, Germany

[4]Department of Biomedical Engineering, Columbia University, New York, New York, USA

[5]Department of Radiology, Columbia University, New York, New York, USA

Correspondence
Michael Hock, Chair of Cellular and
Molecular Imaging, Comprehensive
Heart Failure Center (CHFC), University
Hospital Wuerzburg, Am Schwarzenberg
15, Building A15, D-97078 Wuerzburg,
Germany.
Email: Hock_M2@ukw.de

Funding information
German Ministry of Education and
Research; Grant/Award No. 01EO1504

Purpose: Inhomogeneities of the static magnetic B$_0$ field are a major limiting factor in cardiac MRI at ultrahigh field ($\geq$ 7T), as they result in signal loss and image distortions. Different magnetic susceptibilities of the myocardium and surrounding tissue in combination with cardiac motion lead to strong spatio-temporal B$_0$-field inhomogeneities, and their homogenization (B$_0$ shimming) is a prerequisite. Limitations of state-of-the-art shimming are described, regional B$_0$ variations are measured, and a methodology for spherical harmonics shimming of the B$_0$ field within the human myocardium is proposed.

Methods: The spatial B$_0$-field distribution in the heart was analyzed as well as temporal B$_0$-field variations in the myocardium over the cardiac cycle. Different shim region-of-interest selections were compared, and hardware limitations of spherical harmonics B$_0$ shimming were evaluated by calibration-based B$_0$-field modeling. The role of third-order spherical harmonics terms was analyzed as well as potential benefits from cardiac phase–specific shimming.

Results: The strongest B$_0$-field inhomogeneities were observed in localized spots within the left-ventricular and right-ventricular myocardium and varied between systolic and diastolic cardiac phases. An anatomy-driven shim region-of-interest selection allowed for improved B$_0$-field homogeneity compared with a standard shim region-of-interest cuboid. Third-order spherical harmonics terms were demonstrated to be beneficial for shimming of these myocardial B$_0$-field inhomogeneities. Initial results from the in vivo implementation of a potential shim strategy were obtained. Simulated cardiac phase–specific shimming was performed, and a shim term-by-term analysis revealed periodic variations of required currents.

Conclusion: Challenges in state-of-the-art B_0 shimming of the human heart at 7 T were described. Cardiac phase–specific shimming strategies were found to be superior to vendor-supplied shimming.

KEYWORDS

7 T, B_0, cardiac MRI, shimming, ultrahigh field

1 | INTRODUCTION

Ultrahigh-field MRI promises improved image quality as well as new image contrast for the assessment of the pathophysiology of the heart.[1-3] However, inhomogeneities of the static magnetic field (B_0 field) are a challenge in cardiac magnetic resonance (CMR) imaging at 7 T. Different magnetic susceptibilities of the myocardium, surrounding tissue, and blood in combination with the particular geometrical shape of the heart lead to a complex spatial B_0-field distribution.[4,5] The resulting macroscopic field gradients induce image distortions and lead to significant signal loss in measurements of myocardial microstructure due to a shortened effective transverse relaxation time T_2^*.[6] In addition, cardiac and respiratory motion generate temporal B_0-field variations inside the heart between different cardiac phases and breathing positions.[7] Standard CMR techniques used to assess cardiac function, such as balanced SSFP cine imaging,[8] suffer from these B_0 inhomogeneities, as they create dark band artifacts, but SSFP-based techniques are not widely used at 7 T because of specific absorption rate constraints. Other fast imaging techniques, such as spiral readout trajectories[9] and EPI,[10] also require a homogeneous B_0 field. In particular at 7 T, the peak amplitudes of parallel-transmit RF pulse waveforms and amplitudes are optimized for a certain target range of the B_0-field offset to limit the required RF power and, thus, the specific absorption rate.[11,12] Therefore, the spatial and temporal correction of the B_0 inhomogeneities is of high importance in CMR imaging at 7 T.[13]

The homogenization of B_0 magnetic field distributions is usually referred to as B_0 shimming. Inhomogeneities of the static magnetic field increase linearly with the field strength, making B_0 shimming particularly important for ultrahigh-field MRI. The correcting shim field is typically generated by room-temperature shim coils, which are integrated into the MR system. The coils are located around the bore of the scanner and generate magnetic fields with spatial profiles based on the spherical harmonics (SH) functions.[14,15] Shim systems in clinical 1.5T or 3T MR scanners are usually capable of creating magnetic fields up to the second order of the SH profiles (second-order shims). Based on the measured magnetic field distribution (B_0 map), a driving current is calculated for each shim coil and applied before subsequent measurements to homogenize the B_0 field. Particularly at

7 T, CMR may benefit from higher-order shim coils to compensate for the increased B_0 inhomogeneities compared with lower field strengths. The role of higher order and degree B_0 shimming was described for the human brain at 7 T.[16,17] First-order to third-order shimming resulted in a substantial gain in B_0-field homogeneity over the entire region of interest compared with first-order to second-order shimming. However, such work is missing so far for B_0 shimming of the heart at 7 T, and it needs to be investigated whether higher-order (≥ 3) shims are beneficial for magnetic field homogenization.

There are several methods to map the magnetic field distribution. One-dimensional projection-based techniques measure the B_0 field along specific directions and offer the advantage of short measurement time.[18,19] Projection B_0 mapping is most suitable to compute the SH components of local B_0 fields, which can easily be compensated by first-order and second-order shims.[20] For complex spatial distributions of B_0 inhomogeneities over a large FOV, such as the entire heart, 3D volumetric techniques are another option. One example is the voxel-wise calculation of the B_0 map from the complex phase maps acquired at different TEs of a multi-gradient-echo pulse sequence. Both an appropriate spacing of the TE to obtain a sufficiently large dynamic range of the MR signal, and a sufficiently large SNR at the longest TE are important for this phase method. The approach is used in common shim tools such as customized *B0DETOX*[21,22] software.

So far, the B_0-field inhomogeneities inside the heart have been analyzed at 1.5 T,[23] 3 T,[24] and 4 T.[25] At 7 T, B_0 inhomogeneities were considered both for an optimized saturation pulse train for human first-pass myocardial perfusion imaging,[12] and for the design of parallel-transmit RF pulses robust against respiration in cardiac MRI.[7] However, considerations for cardiac-specific B_0 shimming have only been addressed for 1.5 T and 3 T,[26] and an analysis at 7 T is demanded. B_0-map calculation from phase maps acquired at two TE times, as used in clinical routine at lower field strengths, may be problematic at ultrahigh field due to an increased likelihood of multiple phase wraps, which are problematic to correct unambiguously. In addition, the temporal B_0-field variations between different cardiac phases are not addressed in the standard vendor-supplied B_0-shim protocols. The vendor-supplied shimming is performed for a cuboid-shaped volume, which is typically adjusted to the whole heart.[27,28] However, B_0 shimming targeted to an

anatomy-driven shim region of interest (SROI) improved the field homogeneity in the heart at 3 T.[8,29] The implementation of this approach at 7 T would be a first step toward dynamic shim updating (DSU)[30,31] on subvolumes of the heart, which successfully reduced B_0 inhomogeneities in the brain at 7 T.[16]

This work aimed to assess the spatial and temporal B_0-field variations in the myocardium of the human heart at 7 T. The following challenges for state-of-the-art cardiac B_0 shimming are demonstrated and discussed: (1) the SROI selection, (2) hardware limitations of the SH shim system, (3) the usefulness of third-order SH terms, and (4) potential benefits of cardiac phase–specific shimming (CPSS) (ie, DSU on cardiac phases). A potential shimming strategy is proposed, and its benefits and limitations for successful CMR imaging are discussed.

2 | METHODS

2.1 | Magnetic resonance imaging setup

All measurements were performed on a 7T whole-body MR system (MAGNETOM Terra; Siemens Healthineers, Erlangen, Germany). The scanner was equipped with 80 mT/m gradients and a partial third-order SH shim system; the coils corresponding to the third-order terms Z3, Z2X, Z2Y, and Z(X2-Y2) were available for B_0 shimming, whereas the coils for correcting terms X3, Y3, and XYZ were not implemented. Imaging data were acquired with a 1TX/16RX thorax coil array (MRI Tools, Berlin, Germany). A vendor-supplied multi-gradient-echo pulse sequence in different modifications was then used to measure the field map data.

2.2 | Cardiac triggering

During all in vivo measurements, both the scanner-integrated electrocardiogram and an acoustic cardiac triggering (ACT) system (EasyACT; MRI Tools, Berlin, Germany) were permanently used to monitor cardiac activity.[32] In contrast to the electrocardiogram, the ACT is not affected by magnetohydrodynamic effects and shows no interferences with electromagnetic fields produced by the gradient system. It detects the first heart tone of the phonocardiogram, which corresponds to the closure of the atrioventricular valves at the beginning of systole. For this reason, the ACT was preferred for cardiac triggering according to a previous study,[33] in which ACT was compared with vector electrocardiogram and pulse oximetry triggering in cardiac 2D cine imaging at ultrahigh field. The quality of the ACT signal depends on proper positioning of the stethoscope and could be degraded by potential additional noise interferences and patient breathing.

2.3 | Subject cohort

Eleven healthy volunteers were scanned after the approval of this study by the Ethics Committee of the University of Wuerzburg under application number 7/17-sc. Written, informed consent was obtained from each subject. The first 4 subjects, forming the training group (all female), were 25.0 ± 3.7 years old and had a body weight and height of 57.5 ± 3.7 kg and 165.8 ± 2.6 cm. Subjects 5 to 10, forming the study group (3 female, 3 male), were 23.7 ± 2.7 years old, had a weight of 73.5 ± 15.4 kg, and a height of 176.5 ± 9.4 cm. The eleventh subject scanned to validate the shim strategy was a male with a weight of 78 kg.

2.4 | Scan protocols for in vivo measurements

The training group measurements were performed to set up a scan protocol for the study group, which allowed us to assess the spatial B_0-field distribution across the heart, its temporal variation between systolic and diastolic cardiac phases, and different SROI selections. To assess functions of the heart chambers, CMR images are typically acquired in double-oblique slice orientations. However, arbitrary slice orientations are not supported yet by the software version used for the B_0-field simulation and shim computation. Thus, all data for the B_0-field mapping was acquired with transversal slice orientation.

2.4.1 | Spatial B_0-inhomogeneities

Middiastolic field-map data were acquired at an average trigger delay of 490 ± 66 ms with the following sequence parameters: TE1/TE2/TE3/TE4/TE5 = 1.7/2.8/4.0/6.0/9.7 ms, TR = 401 ms, matrix = 128×128, FOV = 300×300 mm^2, number of slices = 3, slice thickness = 6.0 mm, slice separation = 1.2 mm, flip angle = 25°, GRAPPA = 3, and number of segments = 29. The scan time, which was predetermined by a single breath-hold duration of 15 seconds, limited the data acquisition to a set of three parallel midventricular slices.

2.4.2 | Temporal B_0-field variations between different cardiac phases

The measurement of the B_0 field at various cardiac phases required an adjustment of the sequence parameters such as TR and number of TEs. Field-map data were acquired at eight cardiac phases equally spaced over an average RR interval of 970 ± 127 ms with the following parameters: TE1/TE2/TE3 = 1.7/2.8/4.0 ms, TR = 90 ms, matrix = 128×128,

FOV = 320×320 mm^2, number of slices = 3, slice thickness = 6.0 mm, slice separation = 1.2 mm, flip angle = 40°, GRAPPA = 3, and number of segments = 15. With this parameter set, each slice was measured in a separate breath-hold, resulting in a total net scan time of 45 seconds.

2.4.3 | Selection of shim-region-of-interest

An accurate SROI selection was demonstrated to be advantageous to obtain a homogeneous B$_0$ field within the heart.[8,29] B$_0$ maps were therefore acquired after three adjustments of a transversal SROI cuboid using the vendor-supplied shimming platform: (1) volume-selective shimming covering the entire heart, (2) slab-selective shimming of the three measured slices, and (3) slice-selective shimming of only the central slice. No further anatomy-driven SROI selection was possible here. The vendor-supplied B$_0$ mapping, which was performed in exhaled breath-hold position and without cardiac triggering at the shortest available first TE and interecho spacing,[34] had the following default sequence parameters: TE1/TE2 = 1.02/3.06 ms, TR = 4.3 ms, matrix = 64×64, FOV = 282×282 mm^2, number of slices = 52, slice thickness = 4.4 mm, slice separation = 0.9 mm, flip angle = 4°, GRAPPA = 2, and number of segments = 1.

2.5 | B$_0$-mapping

The B$_0$ maps were reconstructed offline by voxel-wise linear regression of the signal phase evolution over TE in customized *B0DETOX* shim software. Spatial phase unwrapping was performed using an algorithm of the FMRIB Software Library from the Oxford Center for Functional MRI of the Brain.[35] Further analysis, such as calculation of SDs and interquartile ranges (IQRs) of the B$_0$ distributions, was performed in *MATLAB* R2015b (MathWorks, Natick, MA) after the field-map data were exported from the shim software.

Temporal B$_0$-field variations in the left-ventricular and right-ventricular myocardium were quantified as the differences in SDs (ΔSD) and IQRs (ΔIQR) between B$_0$ maps acquired at systolic and diastolic cardiac phases. Here, the IQR represents the difference between the 25th and 75th percentiles of the frequency distribution within a B$_0$ map.

2.6 | Calibration of SH shim system

The B$_0$-field distributions can be decomposed into SH components, and each term in inverse polarity is then required to correct the measured B$_0$-field inhomogeneities. Due to shim-to-shim interactions, each SH component cannot be treated individually, and the shim system calibration is a necessity

for the computation of shim fields and corresponding currents.[16] In addition, the total dynamic ranges (ie, the shim capabilities of each SH-term coil) are derived from the calibration process. The final calibration matrix, which yields all information on the particular SH terms and cross-terms, connects the calculated shim settings with the SH components of the B$_0$ field before shimming and allows noniterative single-step adjustments.

The calibration measurements were performed on a spherical oil phantom using a 1TX/2RX birdcage coil (Siemens Healthineers, Erlangen, Germany). The value of each shim term was varied in seven steps relative to a reference B$_0$ map using 10% of the dynamic range for the linear gradients, and 30% for the higher orders. For each shim setting, the field map data were acquired with the following sequence parameters[36]: TE1/TE2/TE3/TE4 = 1.0/1.3/2.0/4.0 ms, TR = 30 ms, matrix = 108×128, FOV = 186×220 mm^3, number of slices = 64, slice thickness = 2.7 mm, flip angle = 25°, no parallel imaging acceleration was used, and phase maps for each TE were acquired in a single-echo experiment. The total dynamic ranges were: X = 2124 Hz/cm, Y = 2120 Hz/cm, Z = 2129 Hz/cm, X2-Y2 = 6.1 Hz/cm^2, ZX = 12.6 Hz/cm^2, Z2 = 40.2 Hz/cm^2, ZY = 12.3 Hz/cm^2, XY = 6.2 Hz/cm^2, Z(X2-Y2) = 0.10 Hz/cm^3, Z2X = 0.35 Hz/cm^3, Z3 = 0.68 Hz/cm^3, and Z2Y = 0.34 Hz/cm^3.

2.7 | Calibration-based shim-field analysis

The field map data were loaded into the shim software to reconstruct the B$_0$ maps ("measured field map") from the phase maps as described in section 2.5. The anatomy-driven SROI was selected manually on the magnitude images by the user. Afterward, the measured field maps were decomposed into SH components. The computation of the required shim fields was achieved by constrained least-squares fitting using the Levenberg-Marquardt algorithm,[37,38] which was demonstrated to be most robust against changes in the starting-point values in comparison to other generic constrained nonlinear optimization methods.[39] In the least-squares optimization, the resulting shim field could be limited to the dynamic ranges of the shim coils (ie, could be regularized to the hardware capabilities). Based on the determined SH components in the measured field map, a shim field ("simulated shim"), which is necessary to generate the individual field shapes in opposite polarity, and corresponding shim currents were computed.

2.7.1 | Simulation of static shimming

The spatial B$_0$-field distribution in the heart was assessed on middiastolic field-map data to avoid the effect of cardiac

motion resulting from ventricle contraction during the systolic phase.[11] It was evaluated whether the dynamic range of each shim coil was sufficient to compensate for the corresponding SH component by not limiting the currents for the least-squares fitting during magnetic-field modeling. Moreover, the role of the third-order terms was evaluated by simulating three different shims: second order only, second order plus third order taking hardware limitations into account, and second order plus third order not considering those limitations. All three types of shims were simulated based on the unshimmed B_0 field, which was acquired under the system's default shim settings using less than 5% current of the total dynamic range in each coil.

### 2.7.2 | Simulation of cardiac phase-specific shimming

Time-resolved B_0 maps were acquired at eight equally spaced cardiac phases to evaluate the potential of CPSS. After adjusting the SROI and computing the shim settings for a SROI to be updated on each phase, the temporal variation of the individual shim terms was analyzed. Because the current MR system is not equipped with the hardware required for DSU, such as dedicated shim amplifiers, an averaged shim may be useful for cine imaging. This scenario was evaluated by simulating an averaged static shim, which applied the mean of all eight CPSS fields.

2.8 | Implementation of potential shim strategy

A potential shim strategy was developed based on the study group measurements and implemented for in vivo shimming. The strategy consists of the following steps[40,41]:

1. The triggered acquisition of middiastolic B_0 maps for three midventricular slices using ACT;
2. Manual, anatomy-driven SROI selection on the magnitude images in each slice in combination with a voxel-specific field-gradient threshold to exclude outliers;
3. The calibration-based SH B_0-field modeling in dedicated shim software and transformation of the field amplitudes in Hz/cm^n, where n describes the order of the SH shim terms, to shim settings in hardware units; and
4. The application of the computed shim on the MR system and a repetition of step 1 as a control measurement of the B_0 field.

The measured magnitude images and phase maps were transferred from the scanner console to a dedicated workstation and loaded into the shim software. The B_0 maps were
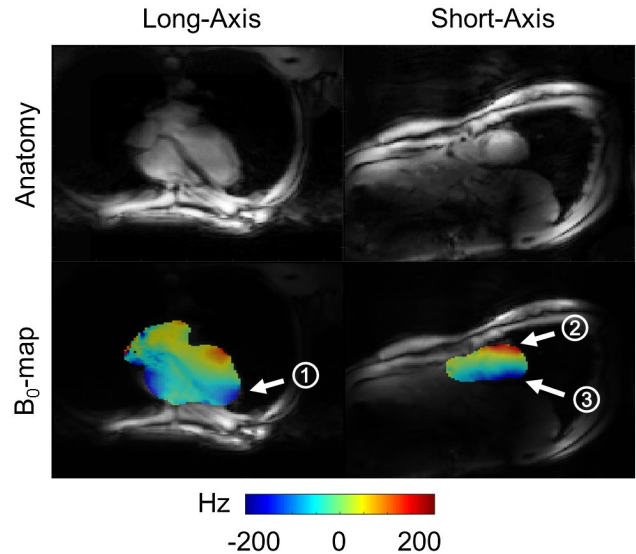
FIGURE 1 Anatomical views of the B_0 distribution inside the heart of a healthy volunteer. In the long-axis view, high negative B_0-field distortions occur near the apex (1). In the short-axis view, high B_0-field inhomogeneities are present at the anterior (2) and posterior (3) part of the left-ventricular myocardium. The windowing of the long-axis and short-axis images was adjusted for visualization using the "adapthisteq" *MATLAB* function, which performs contrast-limited adaptive histogram equalization

reconstructed as described in section 2.5, and an anatomy-driven SROI was selected on the magnitude images by the operator. The computation of the required shim fields and currents was performed as described in section 2.7. The resulting full set of shim settings could be exported from the shim software and be applied at the scanner console. The whole process takes about 6-8 minutes, in which most of the time is required for the manual anatomy-driven SROI selection and application of the shim settings on the scanner console.

3 | RESULTS

The spatial B_0-field distribution inside the heart of a volunteer is shown in long-axis (LA) and short-axis (SA) views in Figure 1. In the LA view, high negative B_0-field inhomogeneities were observed near the apex. In the SA view, high B_0-field inhomogeneities occurred at the anterior and posterior part of the left-ventricular myocardium.

A detailed histogram analysis of the spatial B_0 distribution within the heart showed that most data points were located within −100 Hz to 100 Hz. However, the extreme values were located in localized spots within the left-ventricular and right-ventricular myocardium (Figure 2). The B_0 field in the myocardium showed a temporal variation between systolic and diastolic cardiac phases (Figure 3). In the septum, smaller ΔSD and ΔIQR were observed compared with the rest of the

FIGURE 2 Spatial distribution of the B_0-field inhomogeneities in the heart. Shown are the measured B_0 distributions (left) and corresponding histograms (right) for the entire left ventricle (LV) (A), the left-ventricular myocardium (B), and different segments of the latter (C). Histograms (D)-(F) correspond to the measured B_0-field distributions (A)-(C), respectively. In (F), the color blue corresponds to segment 1, red corresponds to segment 2, yellow corresponds to segment 3, and purple corresponds to segment 4. G, The B_0-field distribution inside the entire right ventricle (RV). Again, the field inhomogeneities of the myocardium (H) are of particular interest and plotted as a histogram (I). In (I), the color yellow corresponds to the anterior segment in (H), blue corresponds to the inferior segment, and red corresponds to the lateral segment
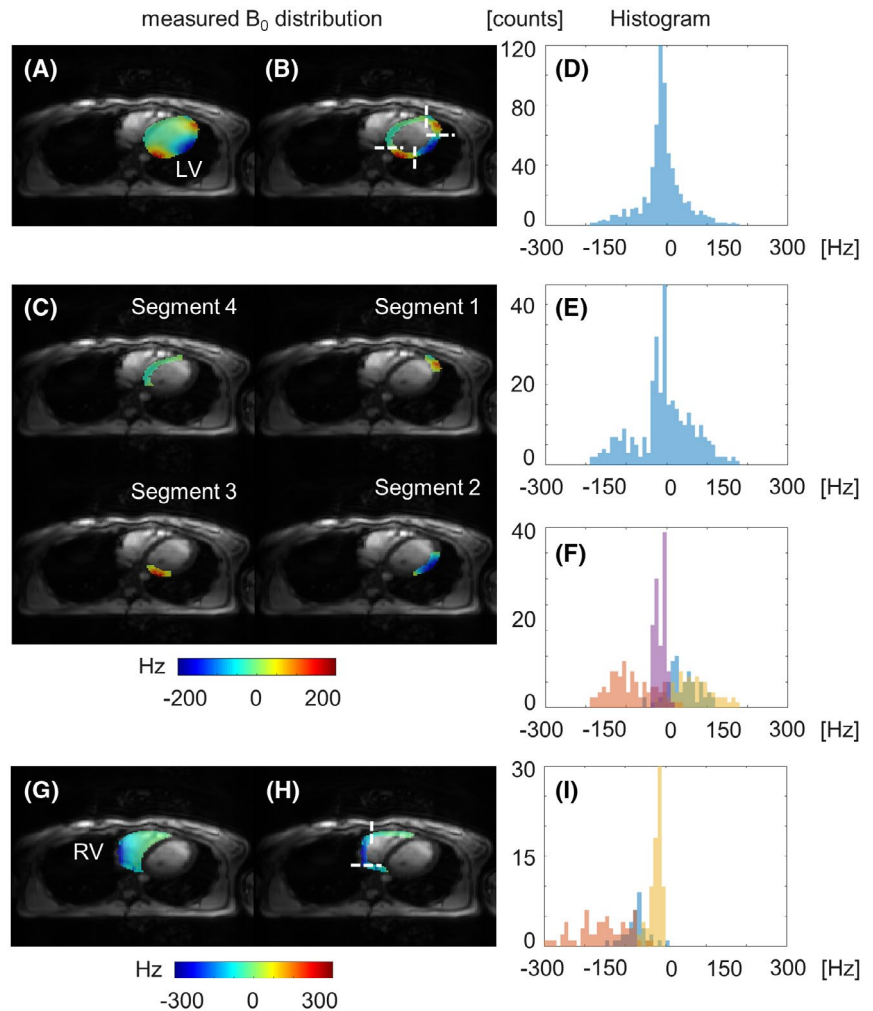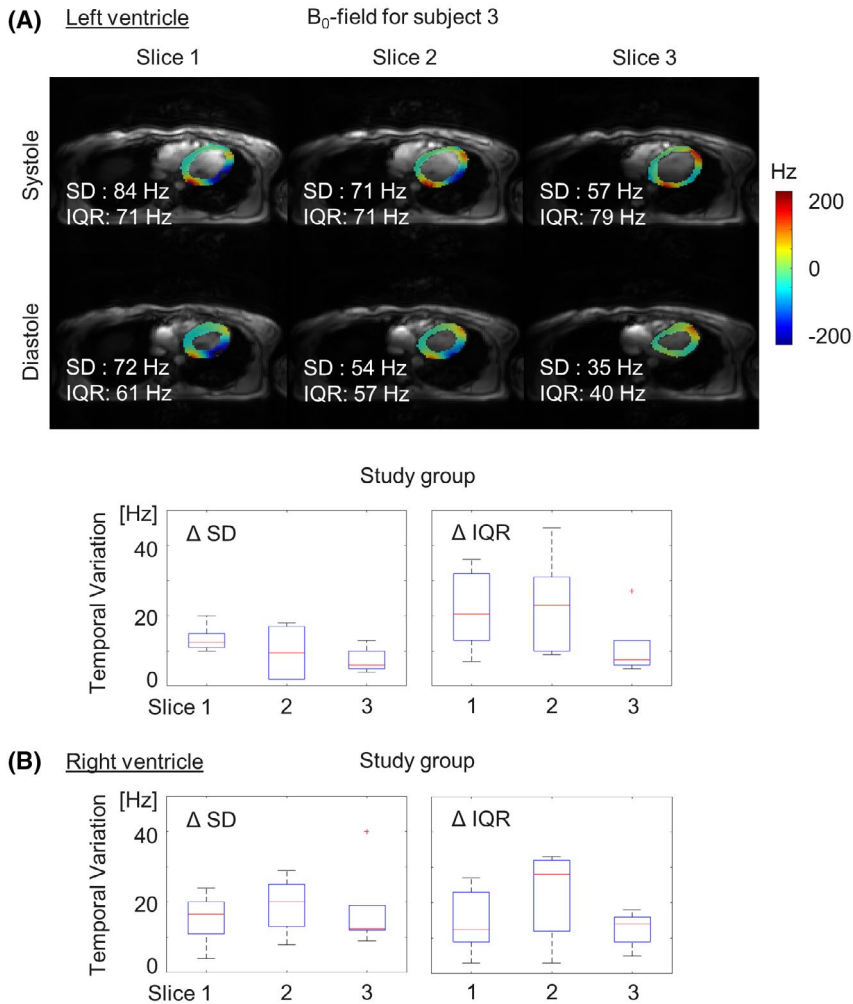

myocardium. The ΔSD in the left-ventricular myocardium also varied from slice to slice (Figure 3A). Averaged over all slices and subjects of the study group, ΔSD accounted for 10 ± 5 Hz and ΔIQR for 19 ± 12 Hz between the same systolic and diastolic cardiac phases, as shown for subject 3. In the right ventricle, ΔSD accounted for 17 ± 9 Hz and ΔIQR for 17 ± 10 Hz averaged over all slices and subjects of the study group (Figure 3B). Within the septum, which was segmented for all subjects as visualized in Figure 2C (segment 4), a temporal B_0-field variation of $\Delta SD_{Sep} = 3 \pm 2$ Hz was observed. Zeroth-order B_0 field (ie, center frequency) changes (ΔF_0) accounted for $\Delta F_{0,LV} = 8 \pm 6$ Hz in the left-ventricular myocardium and $\Delta F_{0,RV} = 16 \pm 11$ Hz in the right-ventricular myocardium across all subjects and slices.

The SROI selection was evaluated from a comparison of B_0 maps measured after applying the volume-selective, slab-selective, and slice-selective vendor-supplied shimming protocol (Figure 4). The slab-selective shimming resulted in a reduced SD and IQR in all three acquired slices, indicating a more homogeneous B_0-field distribution. Throughout the 6 subjects of the study group, the slab-selective shimming reduced the SD of the middiastolic B_0-field distributions by 13 ± 6 Hz and $26\% \pm 11\%$ compared with the volume-selective

shimming (Table 1). However, Table 1 reveals that slice-selective shimming reduced this value further for only 2 subjects.

The field maps measured after the slab-selective shimming revealed the spatial B_0-field distribution within the anatomy-driven SROI (Figure 5A,B). Calibration-based shim field simulations using the proposed shim strategy resulted in predicted B_0-field distributions (Figure 5D), which showed reduced SD and IQR for all subjects compared with the measured field maps. The shim settings for the slab-selective shimming and the simulated shim (Figure 5C) are plotted in Figure 6. The X-gradient, Y-gradient, and Z-gradient offsets showed similar medians for both shims (Figure 6, top row). A comparison of the third-order SH components revealed that the zonal term Z3 showed the largest variation: The median for the slab-selective shimming accounted for 0.06 Hz/cm^3, whereas the median for the simulated shim accounted for -0.58 Hz/cm^3. In 4 of the 6 subjects, simulated shim settings exceeded the maximum of the hardware dynamic range (Figure 6, bottom plot), namely, Z2Y for subject 5, Z3 for subject 7, Z3 and Z2Y for subject 8, and Z3, Z2X, and Z(X2-Y2) for subject 9. A comparison between second order only and second plus third-order shims demonstrated that the

(A) Left ventricle

B_0-field for subject 3

FIGURE 3 Temporal B_0-field variation between systolic and diastolic cardiac phases in the myocardium after volume-selective shimming. The left-ventricular (A) and right-ventricular (B) myocardium were selected similar to Figure 2B,H. For all study group subjects, the differences (ΔSD) between the SDs of systolic and diastolic B_0-field distributions and the differences (ΔIQR) between the corresponding interquartile ranges (IQRs) in (B) were calculated between the same cardiac phases as shown in (A). The red line markers represent the median, and the blue line markers correspond to the 25th and 75th percentiles. The black line markers represent the most extreme data points not considered outliers, and outliers are plotted as a red "+"

third-order terms were particularly beneficial to correct the myocardial B_0 inhomogeneities in the anterolateral segment of the left ventricle (Figure 7). However, residuals of the third-order terms remained due to the hardware limitations of the shim system. The second-order terms did not exceed the hardware limitations for any shim.

The B_0-field distributions measured after volume-selective shimming showed a temporal variation over eight cardiac phases equally spaced by 90 ms (Figure 8A). Reduced B_0-field inhomogeneity was observed after simulation of the averaged static shim (Figure 8B). The B_0-field homogeneity was improved further after simulated CPSS for SROIs updated on each cardiac phase (Figure 8C), which was beneficial for the correction of myocardial B_0 inhomogeneities (Figure 8, cardiac phase 3, white arrows). A detailed analysis of the required CPSS currents revealed a temporal variation of individual shim terms over the cardiac cycle (Figure 8D, red arrows). Across all subjects, CPSS yielded an improvement of ΔSD = 1 $\pm$ 1 Hz in B_0-field homogeneity over the entire heart compared with the averaged static shim. Again, it has to be noted that CPSS was beneficial to reduce myocardial B_0 inhomogeneities, as exemplary shown in Figure 8 for subject 3.

Pilot results of the experimental implementation of the developed shim strategy are shown in Figure 9. Large B_0-field inhomogeneities were observed within the left-ventricular and right-ventricular myocardium before the shim (Figure 9B). The simulated shim is expected to reduce these inhomogeneities significantly (Figure 9D). The experimental shim outcome (Figure 9E) matched the simulated shim outcome and reduced the SD within the SROI from 45-52 Hz slice-to-slice down to 26-33 Hz. However, smaller B_0-field inhomogeneities remain within the myocardium.

4 | DISCUSSION

In this work, the spatio-temporal B_0-field inhomogeneities in the human heart at 7 T were characterized. The extreme values of the B_0-field distribution were located in the myocardium and showed a temporal variation between systole and diastole. Various SROI selections were compared, with the anatomy-driven approach demonstrating improved B_0-field homogeneity in contrast to the standard SROI cuboid. The scanner-integrated third-order SH terms reduced the SD of

(A)
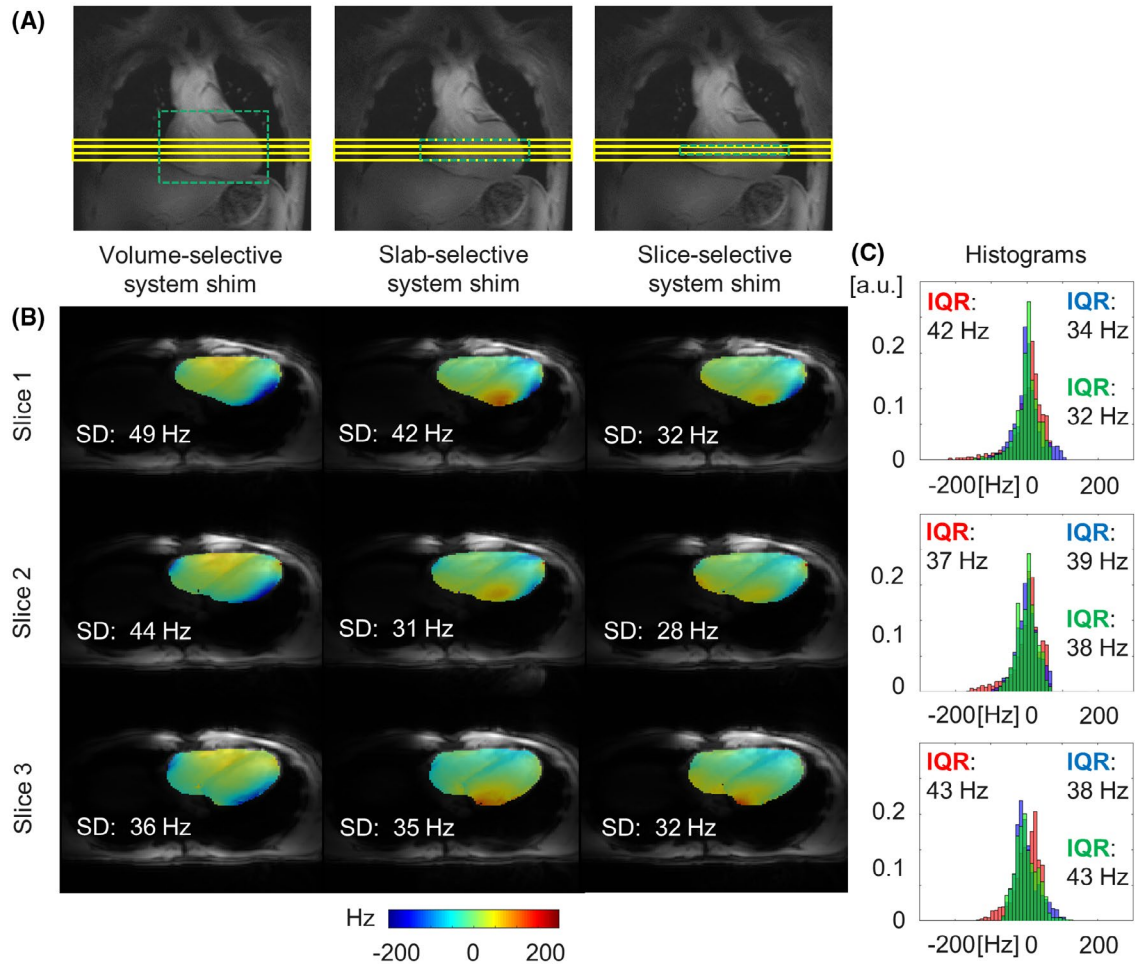
FIGURE 4 Selection of the shim region of interest. A, Schematic views illustrate the selection of the shim region-of-interest cuboid for the vendor-supplied volume-selective, slab-selective, and slice-selective shimming. All three approaches covered all cardiac tissue, but as less surrounding tissue as possible in plane. The measured B_0 fields (B) are shown for subject 7 together with the corresponding histograms (C) obtained after the volume-selective (red bins), slab-selective (blue bins), and slice-selective (green bins) shimming

TABLE 1 B_0-field homogeneity after different vendor-supplied shimming approaches

| Subject	Volume-selective shimming SD (Hz)	Slab-selective shimming SD (Hz)	Slice-selective shimming SD (Hz)
5	42	32	39
6	49	28	54
7	44	31	28
8	66	46	42
9	49	45	49
10	51	39	45

Note: Schematic illustrations of the volume-selective, slab-selective, and slice-selective shimming are shown in Figure 4A. All three shims only differed in the selection of the shim region of interest. The SDs within middiastolic B_0 maps of the heart, as visualized for subject 7 in Figure 4, are given for the central slices.

the B_0 field compared with second order only; however, individual subject-specific third-order terms could not be removed completely due to hardware limitations. Simulated CPSS revealed varying required shim currents on the basis of a shim term-by-term analysis.

4.1 | Spatial B_0-field inhomogeneities

The high B_0-field inhomogeneities in the myocardium were in agreement with earlier studies.[4,12] Their origin was evaluated in previous work by high-resolution simulations
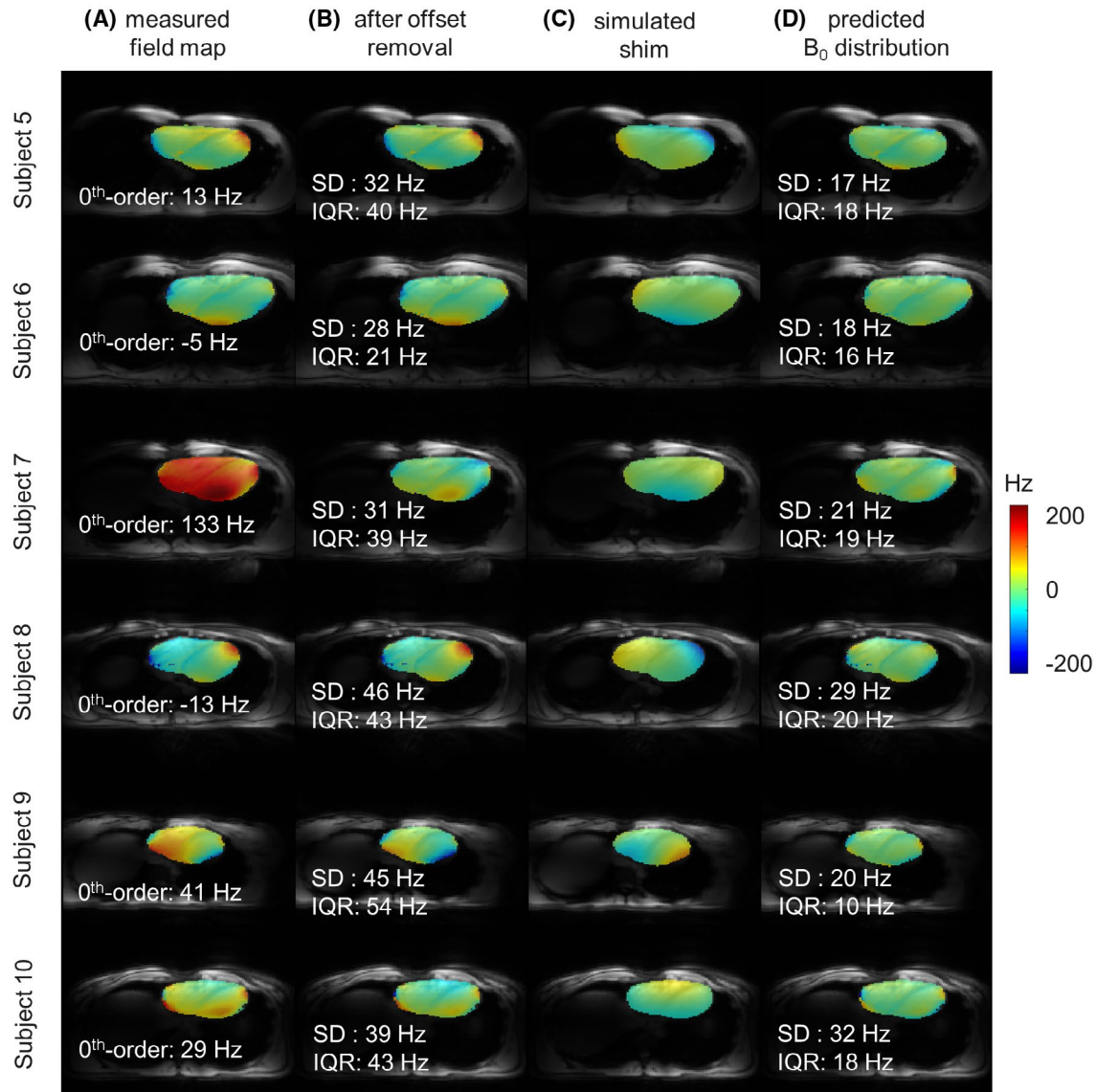
FIGURE 5 Calibration-based shim-field simulations for the B_0 field within the heart. The B_0 fields measured after the vendor-supplied slab-selective shimming as visualized in Figure 4A are shown for the central slices with zeroth-order center frequency ("measured field map") (A) and without ("after offset removal") (B), as well as with the shim fields computed based on the developed third-order shim strategy ("simulated shim") (C) and the expected B_0-field distribution after applying this shim ("predicted B_0 distribution") (D). Note that (C) and (D) refer to an anatomy-driven shim region of interest

of the B_0-field conditions in the human heart, which furthermore showed that typical locations of B_0-field inhomogeneities and dark band artifacts overlap.[42] However, B_0 shimming of the anatomy-driven SA and LA slice orientations was not feasible with the current implementation of *B0DETOX*. In the future, this problem could be resolved by adapting the geometric formalism demonstrated for shimming of single-oblique slices in the brain in the rotations described by the two Euler angles.[43] Another option would be to cover the heart region assessed in the SA and LA orientation by a stack of transversal slices. The anatomy-driven SROI selection could then be performed again in each slice, and a sufficient number of slices would allow us

to shim based on transversal field-map data. However, the slice orientation might result in partial volume effects.[44] To avoid this, an increased slice resolution, and therefore measurement time for the shimming procedure, will be required.

4.2 | Temporal B_0-field variations over the cardiac cycle

The B_0-field distribution within the myocardium changed over the cardiac cycle except for the septum. This is in agreement with earlier studies,[45,46] in which the correlation

FIGURE 6 Comparison of shim settings for the vendor-supplied slab-selective shimming and the simulated shimming shown in Figure 5. A detailed analysis of the scanner-integrated third-order terms is shown in the bottom plot for the simulated shim, where each color presents 1 of the 6 subjects. The black lines mark the hardware limitations of the SH shim system
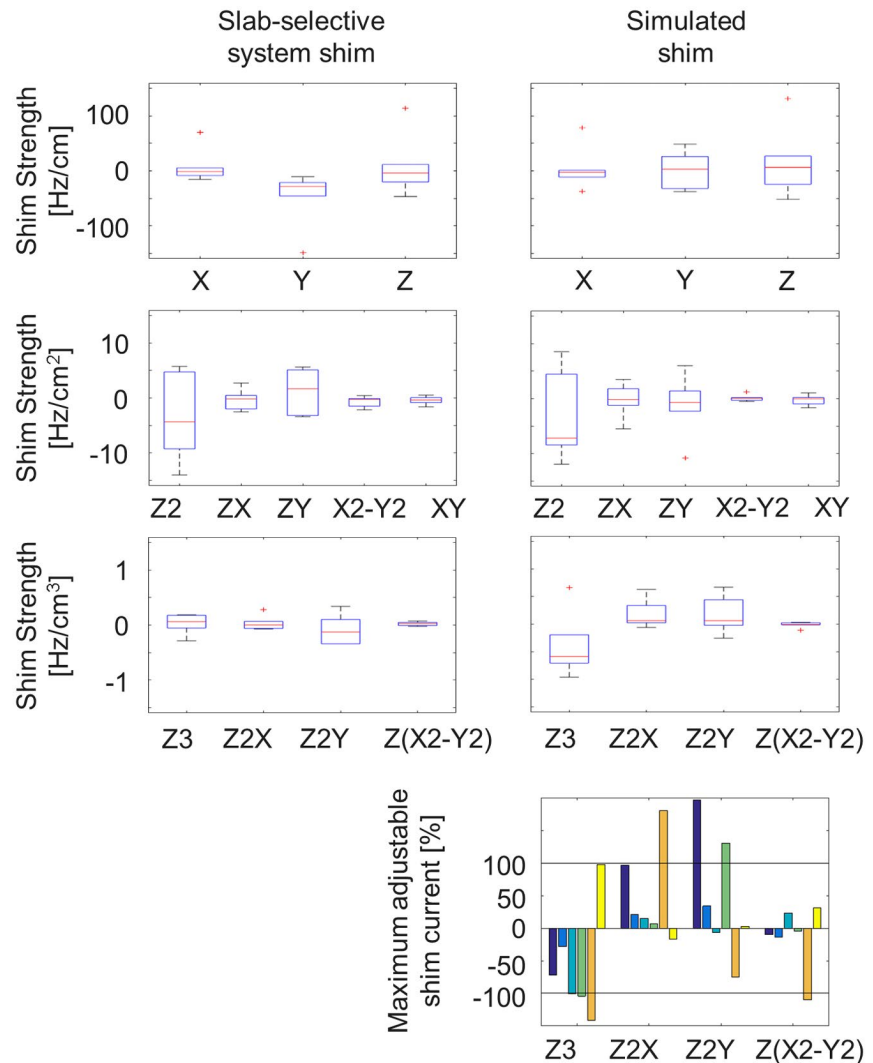
between the myocardial effective transverse relaxation time T_2^* and the left-ventricular wall thickness was examined. The temporal B_0-field variations between systolic and diastolic cardiac phases supported the use of a triggered field-map acquisition. However, no trend was observed for the systolic SD of B_0 to always being larger than the diastolic SD across all analyzed data sets. This might result from the fact that the B_0-field data were acquired in transversal orientation, which leads to strongly subject-specific views. It might be the case that, for example, for SA orientations, either systolic or diastolic SD would always be higher and has to be evaluated when the shim strategy will be tailored to SA and LA views. To overcome the temporal B_0-field variations between different cardiac phases, an earlier study at 3 T demonstrated CPSS for SSFP cine imaging.[47] In the future, the shim settings may therefore be adjusted during systolic and diastolic heart phases for cine imaging.

4.3 | Selection of shim-region-of-interest

Compared with the volume-selective shimming, the slab-selective shimming reduced the cardiac B_0 inhomogeneities significantly. In the latter case, the SROI cuboid had the same height of 18 mm as the stack of measured slices, and in-plane covered the entire heart but as little surrounding tissue as possible. The slice-selective shimming, with the SROI covering the central of the three slices in height but the same in-plane region, resulted in no further reduction of the SD in 4 of the 6 subjects. However, purely transversal slice orientations might result in partial volume effects.[44] Moreover, physiological changes between the acquisition of the initial B_0 map, which forms the basis for the calculation of the shim currents, and the measurement for the evaluation of the shim may have influenced the slice-selective shim results. In this regard, respiration-induced B_0-field variations between different breath-holds are discussed in detail in section 4.4.3.

Simulated shims
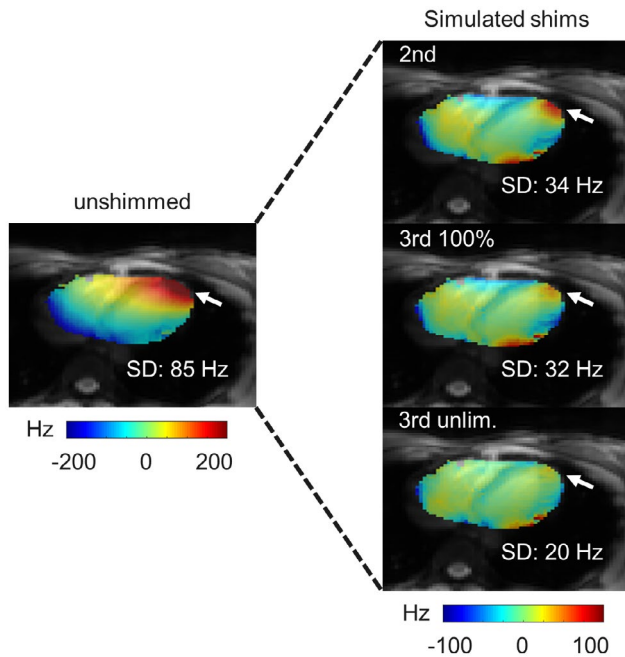
FIGURE 7 Role of third-order terms for B_0 shimming of the human heart at 7 T. Shown is the second-order and third-order shim outcome, in which the third-order shim includes the scanner-integrated spherical harmonics terms Z3, Z2X, Z2Y, and Z(X2-Y2). In addition, the third-order shim was simulated with unlimited dynamic ranges of all shim currents (ie, not taking the hardware limitations of the shim system into account). Note that the unshimmed B_0 field was acquired under default shim settings, which used less than 5% shim strength of the total dynamic range in each coil

This means that the 3D field map should cover an SROI at least one slice thickness (in this case 6 mm) larger in both directions for a reliable shim within it. In-plane shim field simulations showed that an anatomy-driven SROI selection could reduce B_0-field inhomogeneities compared with slab-selective shimming in the shape of a cuboid. In this work, static B_0 shimming was performed. Slab-wise DSU is expected to improve the B_0-field homogeneity inside the heart further.[5]

4.4 | Tailoring the shim strategy

4.4.1 | Hardware limitations of SH shim system

After the partial third-order SH B_0-field modeling, however, localized spots of smaller B_0-field inhomogeneities would remain within the myocardium. The remaining inhomogeneities might result from the hardware limitations of the SH shim system, as the subject-specific shim exceeded the dynamic range of one or more shim coils in some cases. It has to be noted here that for different slice geometries the third-order SH terms might be more or less effective than

for the transversal orientation, and hardware requirements might change consequently. Another reason could be the presence of higher-order SH residuals such as the third-order terms X3, Y3, and XYZ, which are not implemented in the scanner's shim system. The more complex field modeling needed to shim these B_0-field inhomogeneities may be addressed by a dedicated multichannel shim coil approach like DYNAMITE,[21,48] AC/DC,[49] or iPRES.[50] Arranging the shim coils in the same localized setup for all measurements, however, would be more complicated for the heart than for the brain due to different body shapes, and remains the subject for future studies.

4.4.2 | Dynamic shimming

The developed shim strategy is capable of applying a static shim tailored for a certain cardiac phase. However, the MR system used for this study did not support dynamic shimming (ie, slice-by-slice DSU or CPSS) in its current state. Dynamic shimming requires a dynamic shim interface for pre-emphasis and B_0 compensation, as well as dedicated shim amplifiers, to rapidly switch shim currents.[16] To keep updating times for the electronics short, slice-specific or CPSS sets could be stored at the local hardware memory of the dynamic shim interface. Without the possibility of dynamic shimming, a static shim averaged over the cardiac cycle may be an appropriate solution. This may be achieved by monitoring the B_0-field dynamics in terms of optimal CPSS settings and performing an averaged static shim, which applies the mean of all CPSS shim fields. The effect of CPSS on cine imaging could be evaluated by repeating the measurement with a specific trigger delay for each cardiac phase using the corresponding CPSS setting, and therefore without the need for DSU. Note that CPSS might be more or less effective for different slice geometries, making it necessary to repeat the analysis when shim strategies will be tailored for SA and LA orientations.

4.4.3 | Respiration-induced B_0-field variations

The SH terms like X2-Y2 or XY strongly depend on the B_0-field distribution in plane, where the resolution of the measured data was relatively high. The SH components with a significant contribution in z-direction, such as the zonal term Z3, were modeled based on the data in through-slice direction due to the transversal field-map orientation. Here, the number of slices was limited to three within a single breath-hold of 10-15-second duration. An extension of the measurement over multiple breath-holds could result in local respiration-induced B_0 inhomogeneities, which could be investigated by repeating a scan several times over subsequent breath-holds.
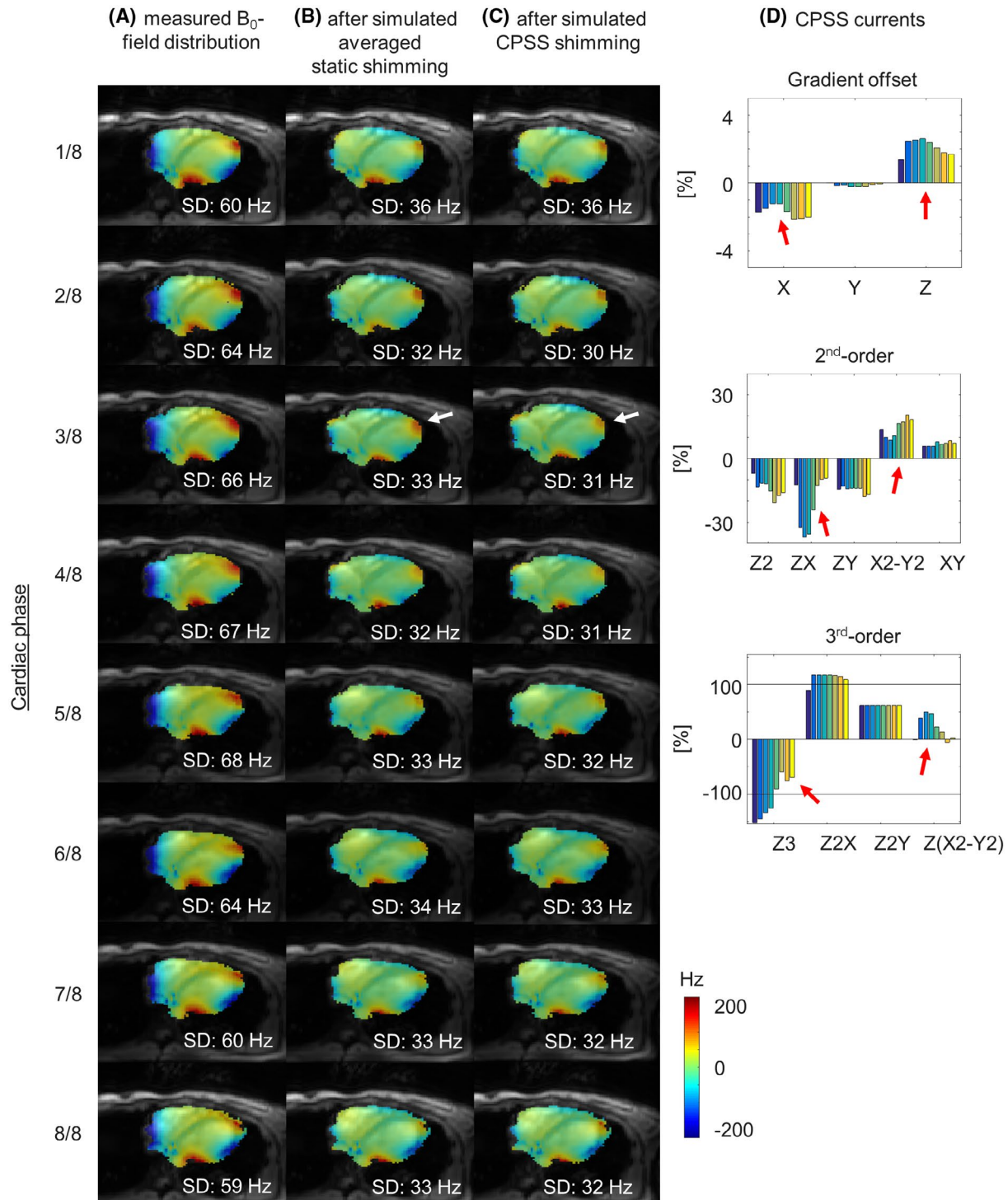
FIGURE 8 Simulation of cardiac phase–specific shimming (CPSS). Shown is the B_0 field within the central slice measured after standard volume-selective shimming (A) and expected after both averaged static shimming (B) and CPSS (C). The CPSS shim currents are visualized in (D), where each color represents an individual cardiac phase. The averaged static shim applied the mean of all CPSS fields

A recent study showed that local B_0 variations approached 100 Hz and more, although the mean value of the B_0 field changed only moderately between exhaled, half-inhaled, and inhaled breath-hold positions.[7] When more slices distributed over several breath-holds have to be acquired, the B_0 maps may in the future be acquired together with diaphragm navigator images, to identify the respiratory position during a calibration scan and apply an appropriate correction. Direct B_0-field monitoring with a field probe and real-time B_0-field updating using a dynamic shim module might be another option and has been demonstrated to reduce respiration-induced field inhomogeneities in the human chest at 7 T.[51]
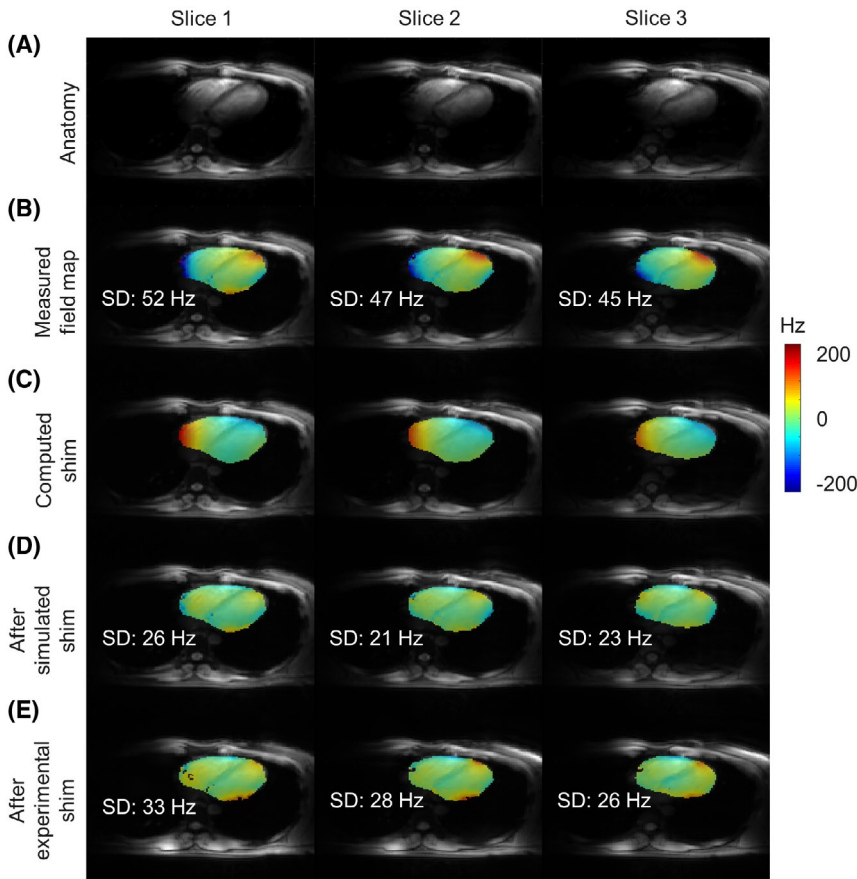
FIGURE 9 In vivo third-order B_0 shimming of the human heart at 7 T. A, The anatomy-driven shim region of interest was selected on the magnitude images. Also shown are the initial measured B_0-field distribution (B), the magnetic shim field computed based on the developed shim strategy (C), the expected B_0-field distribution after the simulated shim (D), and the B_0-field distribution measured after the experimental shim (E). Note that the offset was removed from all B_0-field data

5 | CONCLUSIONS

This work assessed the spatial B_0-field distribution in the human heart at 7 T and its temporal variation in the myocardium between systolic and diastolic cardiac phases. Several challenges for state-of-the-art vendor-supplied shimming methodology, including cardiac triggering and an adequate SROI selection, were demonstrated and discussed. Third-order SH terms were shown to be useful for B_0 shimming of the human heart at 7 T, while subject-specific required shim currents even exceeded the hardware capabilities of the SH shim system. Simulations of CPSS and proof-of-principle in vivo shimming demonstrated a considerable gain in B_0-field homogeneity in comparison to standard static shimming. A potential workflow for CPSS shimming was proposed, and its benefits and limitations were discussed. The presented findings contribute to the development of dedicated shim strategies to correct the B_0 field within the human myocardium. In combination with future technical advances, including shimming of double-oblique SA and LA slice orientations and calibration scans to overcome respiration-induced B_0-field variations, improved CMR imaging at 7 T could be achieved.

ORCID

Michael Hock https://orcid.org/0000-0003-2450-6738

Maxim Terekhov https://orcid.org/0000-0001-5617-7751
David Lohr https://orcid.org/0000-0002-6509-3776
Stefan Herz https://orcid.org/0000-0002-6360-0578
Markus Ankenbrand https://orcid.org/0000-0002-6620-807X
Aleksander Kosmala https://orcid.org/0000-0002-9313-9356
Tobias Gassenmaier https://orcid.org/0000-0002-1089-2036
Christoph Juchem https://orcid.org/0000-0002-1505-201X
Laura Maria Schreiber https://orcid.org/0000-0002-8827-1838

REFERENCES

1. Snyder CJ, DelaBarre L, Metzger GJ, et al. Initial results of cardiac imaging at 7 Tesla. *Magn Reson Med*. 2009;61:517-524.
2. van Elderen SGC, Versluis MJ, Webb AG, et al. Initial results on in vivo human coronary MR angiography at 7 T. *Magn Reson Med*. 2009;62:1379-1384.
3. Thalhammer C, Renz W, Winter L, et al. Two-dimensional sixteen channel transmit/receive coil array for cardiac MRI at 7.0 T: Design, evaluation, and application. *J Magn Reson Imaging*. 2012;36:847-857.
4. Atalay MK, Poncelet BP, Kantor HL, Brady TJ, Weisskoff RM. Cardiac susceptibility artifacts arising from the heart-lung interface. *Magn Reson Med*. 2001;45:341-345.

5. Mattar W, Juchem C, Terekhov M, Schreiber LM. Multi-coil B_0 shimming of the human heart: A theoretical assessment. In: Proceedings of the 24th Annual Meeting of ISMRM, Singapore, 2016. p 1151.

6. Hezel F, Thalhammer C, Waiczies S, Schulz-Menger J, Niendorf T. High spatial resolution and temporally resolved T_2^* mapping of normal human myocardium at 7.0 Tesla: An ultra-high field magnetic resonance feasibility study. *PLoS One*. 2012;7:e52324.

7. Schmitter S, Wu X, Ugurbil K, Van de Moortele PF. Design of parallel transmission radiofrequency pulses robust against respiration in cardiac MRI at 7 Tesla. *Magn Reson Med*. 2015;74:1291-1305.

8. Schär M, Kozerke S, Fischer SE, Boesiger P. Cardiac SSFP imaging at 3 Tesla. *Magn Reson Med*. 2004;51:799-806.

9. Nayak KS, Cunningham CH, Santos JM, Pauly JM. Real-time cardiac MRI at 3 Tesla. *Magn Reson Med*. 2004;51:655-660.

10. Ding S, Wolff SD, Epstein FH. Improved coverage in dynamic contrast-enhanced cardiac MRI using interleaved gradient-echo EPI. *Magn Reson Med*. 1998;39:514-519.

11. Schmitter S, DelaBarre L, Wu X, et al. Cardiac imaging at 7 Tesla: Single- and two-spoke radiofrequency pulse design with 16-channel parallel excitation. *Magn Reson Med*. 2013;70:1210-1219.

12. Tao Y, Hess AT, Keith GA, et al. Optimized saturation pulse train for human first-pass myocardial perfusion imaging at 7T. *Magn Reson Med*. 2015;73:1450-1456.

13. Ferreira PF, Gatehouse PD, Mohiaddin RH, Firmin DN. Cardiovascular magnetic resonance artefacts. *J Cardiov Magn Reson*. 2013;15:41.

14. Golay MJE. Field homogenizing coils for nuclear spin resonance instrumentation. *Rev Sci Instrum*. 1958;29:313-315.

15. Romeo F, Hoult DI. Magnet field profiling: Analysis and correcting coil design. *Magn Reson Med*. 1984;1:44-65.

16. Juchem C, Nixon TW, Diduch P, Rothman DL, Starewicz P, de Graaf RA. Dynamic shimming of the human brain at 7 T. *Concepts Magn Reson B*. 2010;37:116-128.

17. Pan JW, Lo KM, Hetherington HP. Role of very high order and degree B_0 shimming for spectroscopic imaging of the human brain at 7 tesla. *Magn Reson Med*. 2012;68:1007-1017.

18. Gruetter R. Automatic, localized in vivo adjustment of all first- and second-order shim coils. *Magn Reson Med*. 1993;29:804-811.

19. Reynaud O, Gallichan D, Schaller B, Gruetter R. Fast low-specific absorption rate B_0-mapping along projections at high field using two-dimensional radiofrequency pulses. *Magn Reson Med*. 2015;73:901-908.

20. Gruetter R, Boesch C. Fast, noniterative shimming of spatially localized signals. In vivo analysis of the magnetic field along axes. *J Magn Reson*. 1992;96:323-334.

21. Juchem C, Rudrapatna SU, Nixon TW, de Graaf RA. Dynamic multi-coil technique (DYNAMITE) shimming for echo-planar imaging of the human brain at 7 Tesla. *NeuroImage*. 2015;105:462-472.

22. Juchem C. B0DETOX—B0 Detoxification Software for Magnetic Field Shimming. innovation.columbia.edu/technologies/cu173 26_b0detox. 2017. Columbia Tech Venture, license CU17326. Accessed July 8, 2020.

23. Reeder SB, Faranesh AZ, Boxerman JL, McVeigh ER. In vivo measurement of T_2^* and field inhomogeneity maps in the human heart at 1.5 T. *Magn Reson Med*. 1998;39:988-998.

24. Noeske R, Seifert F, Rhein KH, Rinneberg H. Human cardiac imaging at 3 T using phased array coils. *Magn Reson Med*. 2000;44:978-982.

25. Jaffer FA, Wen H, Balaban RS, Wolff SD. A method to improve the B_0 homogeneity of the heart in vivo. *Magn Reson Med*. 1996;36:375-383.

26. Schär M, Kozerke S, Boesiger P. Considerations on shimming for cardiac applications at 1.5 and 3.0 T. In: Proceedings of the 11th Annual Meeting of ISMRM, Toronto, Canada, 2003. p 174.

27. Suttie JJ, DelaBarre L, Pitcher A, et al. 7 Tesla (T) human cardiovascular magnetic resonance imaging using FLASH and SSFP to assess cardiac function: Validation against 1.5 T and 3 T. *NMR Biomed*. 2012;25:27-34.

28. Huelnhagen T, Paul K, Ku MC, Serradas Duarte T, Niendorf T. Myocardial T_2^* mapping with ultrahigh field magnetic resonance: Physics and frontier applications. *Front Phys*. 2017;5:1-19. Article 22.

29. Schär M, Vonken EJ, Stuber M. Simultaneous B_0- and B_1^+-map acquisition for fast localized shim, frequency, and RF power determination in the heart at 3 T. *Magn Reson Med*. 2010;63:419-426.

30. Blamire AM, Rothman DL, Nixon T. Dynamic shim updating: A new approach towards optimized whole brain shimming. *Magn Reson Med*. 1996;36:159-165.

31. Morrell G, Spielman D. Dynamic shimming for multi-slice magnetic resonance imaging. *Magn Reson Med*. 1997;38:477-483.

32. Lohr D, Terekhov M, Kosmala A, Stefanescu MR, Hock M, Schreiber LM. Cardiac MRI with the Siemens Terra 7 T system: Initial experiences and optimization of default protocols. In: Proceedings of the 26th Annual Meeting of ISMRM, Paris, France, 2018. p 3014.

33. Frauenrath T, Hezel F, Renz W, et al. Acoustic cardiac triggering: A practical solution for synchronization and gating of cardiovascular magnetic resonance at 7 Tesla. *J Cardiov Magn Reson*. 2010;12:67.

34. Hock M, Terekhov M, Lohr D, Schröder A, Walles H, Schreiber LM. B0-mapping and shimming efficiency for ex vivo MR imaging of the heart at ultra-high field—validation of standard shimming protocols of MAGNETOM^{TM} Terra 7 T scanner. In: Proceedings of the DGMP and DGBMT Annual Meeting, Dresden, Germany, 2017. p 11.

35. Smith SM, Jenkinson M, Woolrich MW, et al. Advances in functional and structural MR image analysis and implementation as FSL. *NeuroImage*. 2004;23:S208-S219.

36. Hock M, Terekhov M, Lohr D, et al. Calibration of Siemens MAGNETOM™ Terra 7T shim system and analysis of static 3rd-order B_0-shimming of the heart using B0DETOX. In: Proceedings of the 26th Annual Meeting of ISMRM, Paris, France, 2018. p 1752.

37. Juchem C, Nixon TW, McIntyre S, Rothman DL, de Graaf RA. Magnetic field modeling with a set of individual localized coils. *J Magn Reson*. 2010;204:281-289.

38. Juchem C, Herman P, Sanganahalli BG, et al. DYNAmic MultIcoIl Technique (DYNAMITE) shimming of the rat brain at 11.7 T. *NMR Biomed*. 2014;27:897-906.

39. Nassirpour S, Chang P, Fillmer A, Henning A. A comparison of optimization algorithms for localized in vivo B_0 shimming. *Magn Reson Med*. 2018;79:1145-1156.

40. Hock M, Stefanescu MR, Terekhov M, et al. Third-order cardiac B0-shimming at 7 T in humans. In: Proceedings of the ISMRM Workshop on Ultrahigh Field Magnetic Resonance: Technological Advances, Translational Research Promises & Clinical Applications, Dubrovnik, Croatia, 2019. p 3.

41. Hock M, Terekhov M, Reiter T, Lohr D, Juchem C, Schreiber LM. Correction of myocardial B0-inhomogeneities at 7 T with ECG-gated spherical harmonics shimming. In: Proceedings of the 2019 Minnesota Workshop on High and Ultra-high Field Imaging, Center for Magnetic Resonance Research, Minneapolis, MN, 2019.

42. Shang Y, Theilenberg S, Mattar W, et al. High resolution simulation of B0 field conditions in the human heart based on segmented CT images. In: Proceedings of the 27th Annual Meeting of ISMRM, Montreal, Canada, 2019. p 2184.

43. Koch KM, McIntyre S, Nixon TW, Rothman DL, de Graaf RA. Dynamic shim updating on the human brain. *J Magn Reson*. 2006;180:286-296.

44. Attili AK, Schuster A, Nagel E, Reiber JHC, van der Geest RJ. Quantification in cardiac MRI: Advances in image acquisition and processing. *Int J Cardiovasc Imaging*. 2010;26:27-40.

45. Serradas Duarte T, Huelnhagen T, Niendorf T. Assessment of myocardial B0 over the cardiac cycle at 7.0 Tesla: Implications for susceptibility-based cardiac MR techniques. In: Proceedings of the 24th Annual Meeting of ISMRM, Singapore, 2016. p 2541.

46. Huelnhagen T, Hezel F, Serradas Duarte T, et al. Myocardial effective transverse relaxation time T_2^* correlates with left ventricular wall thickness: A 7.0 T MRI study. *Magn Reson Med*. 2017;77:2381-2389.

47. Kubach MR, Bornstedt A, Hombach V, et al. Cardiac phase-specific shimming (CPSS) for SSFP MR cine imaging at 3 T. *Phys Med Biol*. 2009;54:N467-N478.

48. Juchem C, Nixon TW, McIntyre S, Boer VO, Rothman DL, de Graaf RA. Dynamic multi-coil shimming of the human brain at 7 Tesla. *J Magn Reson*. 2011;212:280-288.

49. Stockmann JP, Witzel T, Keil B, et al. A 32-channel combined RF and B_0 shim array for 3T brain imaging. *Magn Reson Med*. 2016;75:441-451.

50. Han H, Song AW, Truong TK. Integrated parallel reception, excitation, and shimming (iPRES) shim. *Magn Reson Med*. 2013;70:241-247.

51. Boer VO, vd Bank BL, van Vliet G, Luijten PR, Klomp DWJ. Direct B_0 field monitoring and real-time B_0 field updating in the human breast at 7 Tesla. *Magn Reson Med*. 2012;67:586-591.